

# TERRAIN MODELING AND AIRBORNE LASER DATA CLASSIFICATION USING MULTIPLE PASS FILTERING

Frédéric Bretar<sup>a,b</sup>, Matthieu Chesnier<sup>a</sup>, Michel Roux<sup>b</sup>, Marc Pierrot-Deseilligny<sup>a</sup>

<sup>a</sup> Institut Géographique National

2-4 Av. Pasteur 94165 St. Mandé cedex, France

Email: {Frederic.Bretar, Marc.Pierrot-Deseilligny}@ign.fr, mchesnier@fr.st

<sup>b</sup> GET-Télécom Paris - UMR 5141 - Département TSI

46 Rue Barrault 75013 Paris, France

Email: Michel.Roux@enst.fr

**KEY WORDS:** Airborne Lidar, Multiple Pass Filtering, ICM, Classification, DTM

## ABSTRACT:

Airborne laser scanner technique provides a 3D perception of the terrestrial topography, including true ground and objects belonging either to vegetated areas or to human made features. The high intrinsic accuracy and regularity of airborne laser sensors makes highly conceivable the extraction of semantic information related to the recorded 3D-points. In this respect, a new algorithm has been developed in order to classify the initial cloud of points into ground/non ground earth points and generate accurate Digital Terrain Models (DTMs) on a regular grid. Our approach is based on a multiple pass classification process. An estimation of the ground is performed within overlapping neighborhood and laser points are classified with regard to this ground estimation. The algorithm moves toward the neighbor where the average altitude is the lowest. We then compare the vicinity of the terrain with the estimated ground and apply a linear correction. As it goes along, points are filtered many times until we vote for the final label. The estimated ground surface is then the input of an energy minimization algorithm (ICM) which consider laser points as a set of attractors. The final DTM will be a trade off between internal properties and its closeness to ground laser points. The resolution may be fine enough to proceed relevant micro relief analysis especially in a rural environment.

## 1 INTRODUCTION

Airborne laser scanner is nowadays a powerful technique for surveying terrestrial landscapes with extremely high accuracy (Bretar et al., 2003). It provides a 3D cloud of points which describe true ground and objects belonging either to vegetated areas or to human made features. These objects can be automatically detected through the so-called filtering processes (Sithole and Vosselman, 2003). Many filters have been developed so far (section 2), but the problem is complex and filters are generally landscape dependent.

We would like to present in this paper an original approach based on a multiple pass filter. The algorithm consists of running through the cloud of points following specific propagation rules, estimating the ground elevation on the fly and classifying neighboring laser points as ground or non-ground ones. The true ground estimation is only an approximation of the final DTM we want to reach. Based on a basic interpolation of this initial surface in order to refine the resolution of the final DTM, we apply a deformable model algorithm considering laser points classified "ground" as local attractors.

After a brief description of different classification approaches, we will describe the algorithm and the final DTM generation process with deformable models. Results will be presented next, before concluding with a discussion about the methodology.

## 2 STATE-OF-THE-ART

### Morphological filters

An effective algorithm for removing non-ground objects is a mathematical morphology filter applied to gray-scale images (DEM). Morphological filtering is based on successive fundamental operations like dilatation, erosion and on combination of them such as opening and closing. Some years ago, over a regular grid (raster format), Kilian (Kilian et al., 1996) proposed to apply

the morphological operator Opening several times with different window sizes starting with the smallest window size over a DEM. Points are successively weighted depending on their belonging to a certain band width higher than the deepest point in the applied window. High weighted points are likely to be ground, whereas low weighted ones are more likely to be non-ground points.

Lohman (Lohman et al., 2000) used a dual-rank morphological filter proposed by Eckstein (Eckstein and Munkelt, 1995). The dual-rank filter initially sorts all gray values with a mask in ascending order and then selects the values that corresponds to a preset rank  $k$ . Interesting results have been derived using this procedure, but a fixed window size cannot fit all non-ground objects.

We may notice now that the morphological approach may be extended to the study of point clouds measured by means of airborne LIDAR. For a LIDAR measurement  $p(x, y, z)$ , the dilation (resp. erosion) of the elevation  $z$  at  $x$  and  $y$  is defined as:

$$d(x, y) = \max_{(x_p, y_p) \in w} (z_p) \text{ and } e(x, y) = \min_{(x_p, y_p) \in w} (z_p) \quad (1)$$

where  $w$  is a planimetric neighborhood of  $(x, y, z)$  and  $(x_p, y_p, z_p)$  is a laser point within  $w$ . The above described dual-rank filter has been improved by Zhang (Zhang et al., 2003) in a progressive morphological filter form. The authors increase (exponentially) the size of the filter and make a series of recursive opening operations. Points are classified as ground if the elevation difference between the laser point at iteration  $k$  and the filtered surface is less than a dynamic threshold that depends on the window size.

### Linear prediction

The linear prediction method (Kraus and Pfeifer, 1998) is based on calculating the distance (residuals) from an average surface to the measurement points. Each  $z$ -measurement is given a weight according to its distance value, which is the parameter of a weight

function. The surface is then recomputed under the consideration of the weights. Intuitively, it is assumed that terrain points are more likely to have negative residuals, whereas vegetation (buildings) points are more likely to have positive residuals. During these iterations a classification is performed. If an oriented distance is above a certain value, the point is classified as off-terrain point and eliminated completely from this surface interpolation. Lee (Lee and Younan, 2003) modified the previous method by implementing an adaptive prediction technique for extracting DTMs of the ground surface underlying vegetation. According to the authors, this technique offers, in general, a better tracking capability in the extraction of bare Earth models with steep slopes and large variability.

### Surface based

An other approach was introduced in (Axelsson, 1999) based on the connection of a surface from below the point cloud. This surface is connected to the ground points using different criteria such as the Minimum Length Description (MDL), constrained spline functions or snakes. All criteria are meant to manage the possible shapes and hence the fluctuations of the resulting surface. The active shape models were first applied to Lidar data in (Elmqvist et al., 2001) and (Elmqvist, 2002). Raw data are first re-sampled over a regular grid, the ground surface is then estimated with the minimization of a defined energy which depends on the internal behavior of the surface, on a data term and on other external forces. According to the author, this algorithm is very robust, and it works on data of different types of terrain.

An other method which is continuously adaptive to terrain surface variations has been developed (Sohn and Dowman, 2002). It aims to recursively divide the LIDAR data into a set of piecewise planar surface models in order to underly terrain slope variations regularized into homogeneous plane terrain. The authors used a downward divide-and-conquer triangulation to run in the point cloud.

### Geometry

The slope-based filter uses the slope of the line between any two points in a point set as the criteria for classifying ground points (Vosselman, 2000). If the slope exceeds a certain threshold then the highest point is assumed to belong to an object. This filter was modified so that the threshold should vary with respect to the slope terrain (Sithole, 2001).

## 3 DESCRIPTION OF THE ALGORITHM

The algorithm is based on a bipartite *voting* process. A laser point will be labeled several times either as ground or non-ground points until the most represented label be affected to the final classified point. Following the propagated direction (section 3.1), an estimation of the ground is performed (section 3.2). This prime DTM is then refined by using an energy minimization algorithm so that the final DTM should be as accurate as we may expect from laser data.

### 3.1 Propagation

The propagation mechanism consists of moving onto a regular geocoded grid. Starting from the cell whereupon the lowest laser point is included, the algorithm explores his 4 *non-visited grid* neighbors (4-connectivity). It then extracts the corresponding *laser* neighbors  $V$  (equation 2) and insert both their average altitude and their position in a sorted (ascending order) container structure.

$$V = \{l_k = \begin{pmatrix} x_k \\ y_k \\ z_k \end{pmatrix} \}_{k \in \mathbb{N}} / \left\{ \begin{array}{l} |x_{center} - x_k| \leq C \\ |y_{center} - y_k| \leq C \end{array} \right\} \quad (2)$$

where  $l_k$  is a laser point,  $(x_{center}, y_{center})$  is the planimetric center of the neighborhood and  $C$  is a constant. The algorithm propagates itself toward the lower feature of this structure. Figure 1 sketches the behavior of the propagation: black cells have already been visited whereas gray ones are potential candidates.

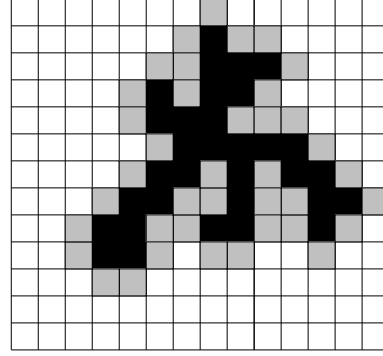


Figure 1: Aspect of the propagation on a geocoded grid. Black cells have already been visited whereas gray ones are potential candidates

### 3.2 Segregating bare/non-bare earth points

How a laser point is **temporary** classified as a terrain point? An altimetric difference is calculated between the  $z$  component of the laser point and the estimated terrain elevation at this place ( $\hat{Z}_{ground\ local}$ ). This estimation is a mean of the 20% lowest laser points of the neighborhood. If the difference is less than a fixed threshold (say  $50cm$ ), the point is considered to belong to the terrain. A new estimation of the terrain height is then computed (mean of points classified as ground) taking into account the new ground laser point. If the difference is larger, the point is classified as a non-ground point. This calculation is performed until all laser points belonging to  $V_{i,j}$  ( $(i, j)$  are the coordinates of the geocoded grid) be processed. A prime DTM (denoted  $\mathcal{S}_{in}$  in this paper) is then filled at  $(i, j)$  with the ground value  $\hat{Z}_{ground\ local}$ .

The algorithm has its own error self detector which will underline both erroneous ground estimations and 3D-point misclassification. This detector is based on the comparison between the average local elevation of the ground  $\bar{Z}_{ground\ local}$  of  $\mathcal{S}_{in}$  ( $3 \times 3$  window size without the central cell, see Figure 2(a)) and the above calculated  $\hat{Z}_{ground\ local}$ . A point classified as ground will be detected if the local slope is larger than  $\arctan \frac{\Delta h}{R}$ , where  $R$  is the resolution of  $\mathcal{S}_{in}$  and  $\Delta h$  is the altitude difference. We therefore apply a linear correction (equation 3) to the current ground elevation in order to take into account the *real* local slope.

$$\hat{Z}_{ground\ local} \leftarrow \alpha \hat{Z}_{ground\ local} + (1 - \alpha) \bar{Z}_{ground\ local} \quad (3)$$

where  $\alpha$  a constant chosen depending on the respective weight we want to grant either to  $\bar{Z}_{ground\ local}$  or to  $\hat{Z}_{ground\ local}$ .

Considering the overlapping structure of our neighborhoods, laser points are classified several times (exactly  $(\frac{C}{R})^2$ ). As we can see on Figure 3,  $V_{i,j}$  and  $V_{i+1,j}$  have a large number of common points (empty circles). As a result, for each neighborhood extraction, points will be labeled following local criteria. At the end of the propagation, a laser point will have been labeled  $p$  times as ground and  $n$  times as non-ground. We then affect the final label corresponding to  $\max(n, p)$ , which is the most representative vote.

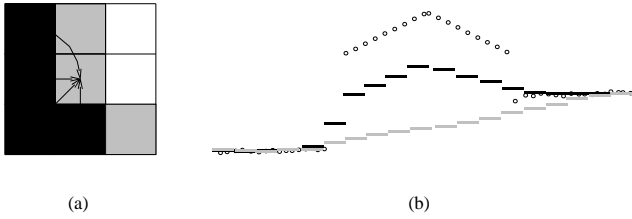


Figure 2: (a) Black cells have already been visited whereas gray ones are potential candidates for propagating (see Figure 1).  $\bar{Z}_{ground\ local}$  is calculated by averaging elevation over black cells. (b) Illustration of the linear correction. Empty circles are laser points. Black dash lines are the estimated local ground  $\hat{Z}_{ground\ local}$  **without** linear correction whereas gray dash lines are the estimated local ground  $\hat{Z}_{ground\ local}$  **after** linear correction

### 3.3 Post-processing

Let us introduced now an intermediate class called low non-ground points. This class is a buffer with low vegetation features, cars and sparse medium height micro-relief. A laser point  $pt$  belongs to this class if  $pt.z \in [S_{in} + \sigma, S_{in} + 2m]$  where  $\sigma$  is the tolerance on ground points. The next step of our algorithm consists of an iterative convergence toward a stable state of  $S_{in}$  whereupon laser points will change their label depending on this belonging to this intermediate class. Point label may change and  $S_{in}$  is updated. The process carries on until convergence of the algorithm (no longer label movement).

The last step consists of comparing the classified point cloud with the final DTM (after deformation, section 3.4). Points lower than  $S_f + 0.5m$  belong to the ground.

### 3.4 Deformable Model

The estimated ground surface  $S_{in}$  is of importance for classifying laser points: the more accurate the surface, the more relevant the classification. Nevertheless, the multiple pass filter will force the continuity of the ground estimation. Topographic details will therefore be smoothed (80% overlapped neighborhood) sidestepping major ground descriptive laser points. Seeing that surveying micro relief is a major characteristic of airborne laser technology, it is necessary to take these points into account when estimating the true ground surface. Secondly, the resolution of this surface is coarse mainly for computing time efficiency. Considering laser performances, we may fairly expect to have a final high resolution DTM with a micro detail description (modulo the point density). We will therefore consider this surface  $S_{in}$  as an initial input of a deformable model algorithm.

This method has similarities with active shape models, but we will consider attractors belonging *exclusively* to the ground (following criteria of the classification algorithm). We will not describe in this paper the whole theoretical framework of deformable models (Montagnat et al., 2000) (Fua and Leclerc, 1994) (Fua, 1997) (Metaxas and Kakadiaris, 2002), but only the main hypothesis and the functions we used for airborne laser applications.

The energy of a deformable model is composed of several terms including at least an intrinsic regularizing term  $\mathcal{E}_{reg}$  and a data term  $\mathcal{E}_{ext}$ . The energy of the surface  $\mathcal{S}$  is defined by:

$$\mathcal{E}(\mathcal{S}) = \mathcal{E}_{reg}(\mathcal{S}) + \mathcal{E}_{ext}(\mathcal{S})$$

Note that  $\mathcal{S}$  must belong to the set of square integrable functions,

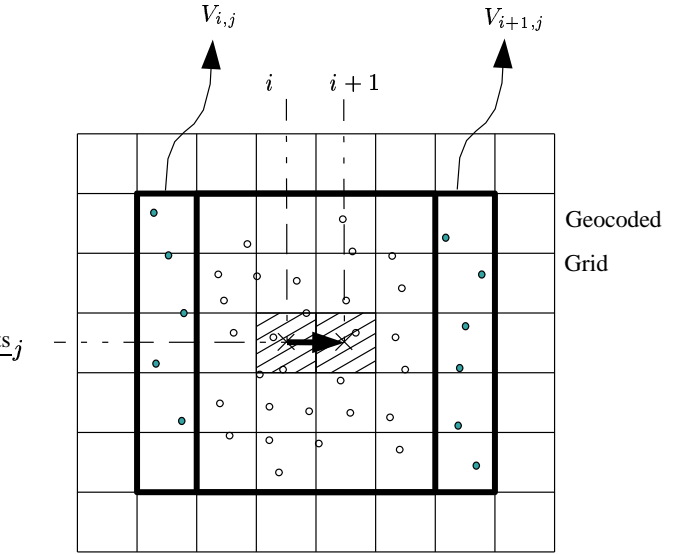


Figure 3:  $V_{i,j}$  represents the neighborhood at grid cell  $(i, j)$  whereas  $V_{i+1,j}$  is the next neighborhood extraction following the propagation route. Empty circles are common laser points, which will be consecutively processed. The ground estimation is performed onto  $S_{in}(i, j)$ ,  $S_{in}(i + 1, j) \dots$  using points classified as ground within a laser neighborhood  $V_{i,j}$ ,  $V_{i+1,j} \dots$

and be twice differentiable. We admit that the energy functional is built such that its global minimum coincide with the expected solution  $\mathcal{S}_f$ :

$$\mathcal{S}_f = \min_{\mathcal{S}} \mathcal{E}(\mathcal{S})$$

The regularizing term has a stabilizer role since the data term is usually very irregular and shows a large amount of local minima. In our implementation,  $\mathcal{S}_f$  is approximated by the minimum of equation 4:

$$\mathcal{E}(\mathcal{S}) = \sum_{i,j} \min_{\mathcal{S}_n} \left( \mu_1 \mathcal{E}_{ext}^{(i,j)}(\mathcal{S}_n) + \mu_2 \mathcal{E}_{reg}^{(i,j)}(\mathcal{S}_n) \right) \quad (4)$$

We used an Iterated Conditional Modes (ICM) algorithm (Li, 1995) (Zinger et al., 2002) for computing a local minimum. In this context,  $\mathcal{S}$  is discretized over a regular grid. The grid nodes  $(i, j)$  are the movable DTM values. For each grid node, the cost function is calculated for a large set of quantified values the surface can have. We then attributes to the grid node the value which minimizes the cost function. 3D laser points are treated as attractors and we define the data local energy  $\mathcal{E}_{ext}^{(i,j)}(\mathcal{S}_n)$  of  $\mathcal{S}_n$  by

$$\mathcal{E}_{ext}^{(i,j)}(\mathcal{S}_n) = \begin{cases} \left( \mathcal{S}_n(i, j) - z_a^{(i,j)} \right)^2 & \text{if } z_a^{(i,j)} \text{ exists,} \\ 0 & \text{if not.} \end{cases} \quad (5)$$

which is the Euclidean distance between the actual surface  $\mathcal{S}_n$  and the corresponding orthogonal laser attractor  $z_a^{(i,j)}$ . Within the ISM algorithm, the minimization is performed over the following values of  $\mathcal{S}_n$

$$\begin{aligned} \mathcal{S}_n(i, j) &= \mathcal{S}_{n-1}(i, j) + \delta z \quad n_0 \leq n \leq n_{max} \\ \text{with } \mathcal{S}_{n_0}(i, j) &= \min(z_a^{(i,j)}, \mathcal{S}_n^{k-1}(i, j)) \\ \mathcal{S}_{n_{max}}(i, j) &= \max(z_a^{(i,j)}, \mathcal{S}_n^{k-1}(i, j)) \end{aligned} \quad (6)$$

where  $\delta z$  is a constant and  $\mathcal{S}_n^{k-1}$  is the value of  $\mathcal{S}_n$  at the  $(k-1)$ th iteration of the process.

The regularization term  $\mathcal{E}_{reg}^{(i,j)}(\mathcal{S}_n)$  approximates the curve's tension and the sum of the square of the curvatures

$$\mathcal{E}_{reg}^{(i,j)}(\mathcal{S}_n) = \left( \frac{\partial \mathcal{S}_n}{\partial x} \right)_{(i,j)}^2 + \left( \frac{\partial \mathcal{S}_n}{\partial y} \right)_{(i,j)}^2 + \left( \frac{\partial^2 \mathcal{S}_n}{\partial x^2} \right)_{(i,j)}^2 + \left( \frac{\partial^2 \mathcal{S}_n}{\partial y^2} \right)_{(i,j)}^2 + 2 \left( \frac{\partial^2 \mathcal{S}_n}{\partial x \partial y} \right)_{(i,j)}^2 \quad (7)$$

Partial derivatives are calculated using centered finite differences.

#### 4 THE DATA SETS

This algorithm has been tested with various LIDAR systems. The scan mechanism of TopoSys is based on a fixed glass fiber array. Its specific design produces a push-broom measurement pattern on the ground. TopoSys data were acquired both from an airplane and an helicopter vector. The data set over Roujan, South of France, corresponds to the last recorded pulse. The ground is more likely visible with this pulse. But the first echo was used over the city of Amiens (there was not any vegetation in the test area). On the contrary, the ALS40 works with a rotating mirror, providing an entirely different ground pattern.

Table 1 gathers the main information about the different LIDAR data sets.

Test Area	Amiens	Roujan	Montmirail
Height (m)	1005	900	3000
System	TopoSys	TopoSys	ALS40
Vector	Plane	Helicopter	Plane
Density (pt/m <sup>2</sup> )	7.5	26.8	0.07
Landscape	City	rural	mountain
Extension	0.64 km <sup>2</sup>	0.2 km <sup>2</sup>	36.8 km <sup>2</sup>
Nb of pts	3.10 <sup>6</sup>	4.10 <sup>5</sup>	4.10 <sup>5</sup>

Table 1: Overview of the test data sets

Moreover, various landscapes (city centers, rural landscapes, forested and mountainous areas) were processed in order to have a large overview of the algorithm behavior.

#### 5 RESULTS

The initial surface  $\mathcal{S}_{in}$  was computed within a  $3m \times 3m$  grid size. Nevertheless, as mentioned before, we did refined the resolution applying a simple Nearest Neighborhood interpolator so that the final resolution should be  $0.5 m$ . In order to make this surface twice differentiable, we did apply a weak gaussian filter before computing the energy minimization algorithm. Laser data over Roujan and Montmirail have been processed with a  $15m \times 15m$  square neighborhood, whereas we used a  $20m \times 20m$  square neighborhood for Amiens.  $\alpha$  was set up to  $\frac{1}{4}$ .

Figure 4 shows laser points (green) classified as non-ground points projected onto an aerial image acquired over the city of Amiens. The result of the classification clearly shows that within this dense urban area, all buildings have been detected as well as small inner courtyards. Since both laser and image surveys have not been acquired in the same time, mobile objects may not fit. Even if it is not depicted on the Figure 4 for readable concern, cars are classified as low non-ground points.



Figure 4: Laser points (in green) classified as non-ground points projected onto an aerial image (20 cm resolution) over the city of Amiens, France.

Figure 5 presents a 3D-view of a classified laser landscape over the area of Roujan. The high point density of this data set (26.8 pt/m<sup>2</sup>) allows us to detect micro-relieves with a good accuracy. We can point out the regular pattern of the low non-ground class such is vineyard in this case. Small copse (red) have also been detected. White points belong to the ground. Even if the second laser echo has been used here, we may notice that ground is not seen everywhere on the scene: last pulse does not penetrate dense canopy.

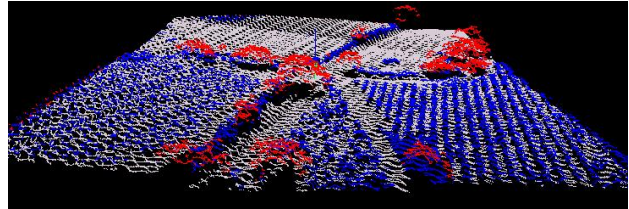


Figure 5: 3D view of a classified laser landscape over the area of Roujan, France. White, blue and red points are respectively ground, low non-ground and non-ground laser points.

In order to have a more detailed description of the results, we present in Figure 6 a profile of both the final DTM (in gray) and the classified laser points over an other location of the Roujan data set. Low non-ground points (blue) are mainly vineyard whereas non-ground points (green) are vegetation. After 15 iterations, the deformable model algorithm found the best surface (fitting our criteria). The calculated DTM (with a  $0.5 m$  resolution) describes a relevant micro topography, even where laser points are missing.

Figure 7 shows the prime terrain estimation  $\mathcal{S}_{in}$  (black line) over the same profile as in Figure 6. The final DTM (gray lines) shows the refinement after the processing of the deformable model algorithm.

The algorithm works with various laser data (see Table 1). Figure 8 shows the resulting DTM of a large scale laser survey (36.8 km<sup>2</sup>) with a low point density over the mountainous area of Montmirail, South of France. What is of importance in this result is the capability of the algorithm to compute a large amount

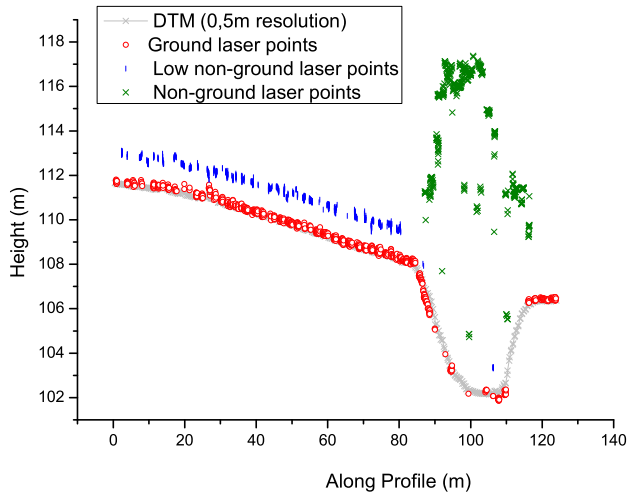


Figure 6: profile of both the final DTM (in gray) and the classified laser points over an other location of the Roujan data set. red circles, vertical blue dashes and green crux are respectively ground, low non-ground and non-ground laser points.

of laser data (more than  $3.10^6$  points). The propagation mechanism efficiency is directly linked to the point density and as a result to the neighborhood dimension.

## 6 DISCUSSION

The algorithm presented in this paper classifies raw laser data into three classes: ground, non-ground, and an intermediary one with points that could belong to one of the previous ones. We did focus on the quality of the resulting classification as well as on the accuracy of the DTM. Unfortunately, we did not have *in situ* measurements for any of the laser data sets we tested. As a result, ground is estimated only with regard to laser points and it was not possible at the time of this study to provide any index of the classification quality. But we planned to compare classification results over urban areas with the related cadastral map.

As far as the classification part is concerned, we may point out interesting behaviors of the algorithm. At first, the lower bound of the low non-ground class influences the final 3D point label. This parameter can be tuned with an a priori knowledge of the landscape composition (in a urban environment, cars (low non-ground) are generally lower than  $1.5\ m$  whereas in a rural area, non-ground vegetation begins  $20\ cm$  over the ground). It is of importance because points classified as low non-ground ones will not be considered to be attractors when it comes to compute the deformable model. Therefore, the final DTM will not be as accurate as it should have been.

Secondly, the ground estimation is performed using a set of laser points included into a defined neighborhood. The shape of this neighborhood do not influence the classification. But for maximizing the continuity of the initial surface, the overlapping ratio must be large enough (up to 70%). The neighborhood size must take into account the point cloud density ( $card(V) > 20\ pts$ ) as well as local variations of the topography ( $C < 20\ m$ ). It is always better when a real ground point is included into the neighborhood since laser points will be classified with regard to computed ground points and propagated neighboring values.

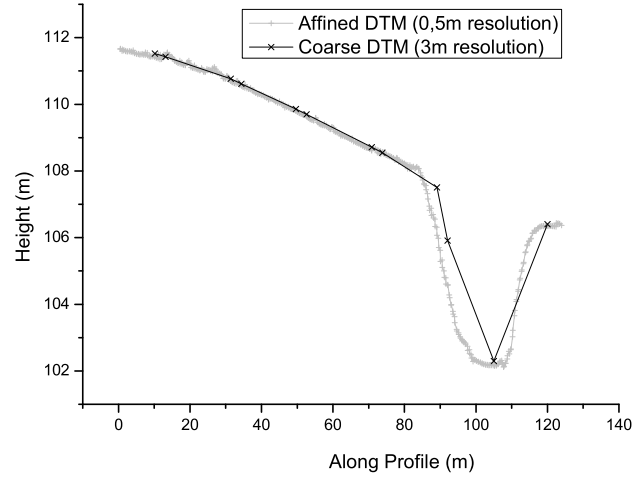


Figure 7: Black line depicts  $S_{in}$  (DTM after the classification process). Gray line is the final DTM at the top end of the process.

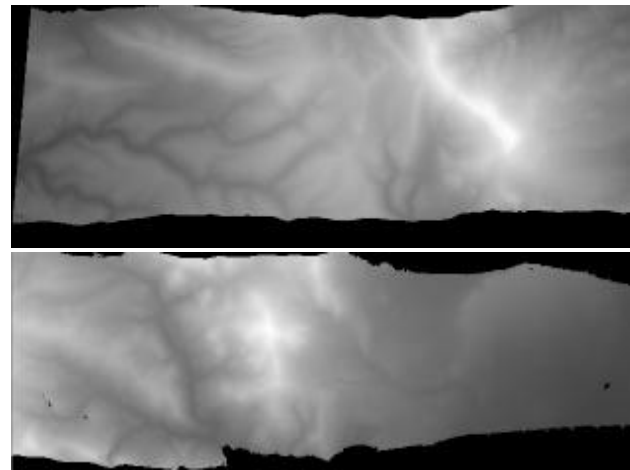


Figure 8: Resulting  $0.5\ m$  resolution DTM of the classification of a mountainous area near Montmirail, South of France. These two pictures represent the same laser strip split up for the presentation concerns. It is a  $16\ km$  long and  $2.3\ km$  wide strip.

As a matter of course, the ICM algorithm will not make the curve converge toward a global energy minimum. But we must keep in mind that the laser point is already an integration of the real backscattered energy of the laser impact. Therefore, the resulting punctual altitude is slightly noisy and the final attractors may not belong exactly to the true ground. We thereafter just need to compute a local minimum energy associated to the final bald Earth model.

The propagation strategy ensures a coherent diffusion of the altitude information. As it is presented in Figure 9 right (Amiens), roads are first computed following the lowest neighboring average altitude, then buildings are tackled. The chosen route depends on the initial seed. It is an on-going development to check the discrepancies of two point clouds classified from a different starting point.

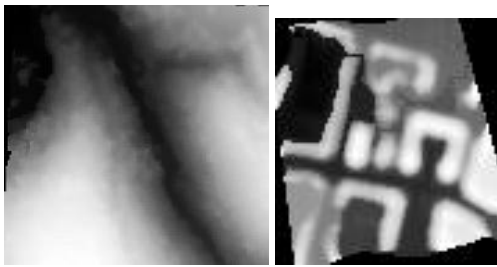


Figure 9: Aspect of the propagation mechanism over a valley in Montmirail (left picture) and Amiens (right picture). The processing time is coded in a gray level scale: first to last point processed (black to white)

## 7 CONCLUSION AND FUTURE WORK

We have presented in this paper an efficient algorithm for classifying a cloud of 3D points. This classification divides laser points into three main classes: ground, low non ground and non ground points. When performing the classification, an initial estimation of the ground is calculated. This surface is then the input of a deformable model algorithm. The final DTM may have a very high resolution, and bring to the light relevant geomorphological features such as of special interest for hydrological applications.

In a near future, we will focus our researches toward two particular points:

- i. finding automatically the optimal neighborhood size depending on the point density.
- ii. going further into the classification process, that is studying more precisely the non-ground class. With laser multiple echoes, and a local statistical approach, vegetation can be separated from buildings. We may think as well of using intensity measurements for clustering points within the classified point cloud as well as optical images.

We would like at last to test this algorithm over photogrammetric derived Digital Elevation Model, since entirely automatic methods do not work properly for extracting non-ground points.

## 8 ACKNOWLEDGMENTS

The authors would like to thank the *Maison de la télédétection*, affiliated to the French institute for water resources (CEMAGREF) in Montpellier, France, for providing laser data over Roujan as well as scientists of the MATIS laboratory for all fruitful discussions we had together.

## REFERENCES

Axelsson, P., 1999. Processing of laser scanner data - algorithms and applications. *ISPRS Journal of Photogrammetry and Remote Sensing* 54, pp. 138–147.

Bretar, F., Pierrot-Desseilligny, M. and Roux, M., 2003. Estimating intrinsic accuracy of airborne laser data with local 3D-offsets. Vol. XXXIV, *International Archives of Photogrammetry and Remote Sensing*, Dresden, Germany, pp. 20–26.

Eckstein, W. and Munkelt, O., 1995. Extracting objects from digital terrain models. Vol. 2572, *Proc. Int. Society for Optical Engineering: Remote Sensing and Reconstruction for Three-Dimensional Objects and Scenes*.

Elmqvist, M., 2002. Ground surface estimation from airborne laser scanner data using active shape models. Vol. XXXIV part

3A, *International Archives of Photogrammetry and Remote Sensing*, pp. 114–118.

Elmqvist, M., Jungert, E., Lantz, F., Person, A. and Soderman, U., 2001. Terrain modelling and analysis using laser scanner data. Vol. XXXIV part 3/W4, *International Archives of Photogrammetry and Remote Sensing*, pp. 219–226.

Fua, P., 1997. *RADIUS: Image Understanding for Intelligence Imagery*. Morgan Kaufmann, chapter Model-Based Optimization: An Approach to Fast, Accurate, and Consistent Site Modeling from Imagery.

Fua, P. and Leclerc, Y. G., 1994. Using 3-dimensional meshes to combine image-based and geometry-based constraints. In: *ECCV* (2), pp. 281–291.

Kilian, J., Haala, N. and Englich, M., 1996. Capture and evaluation of airborne laser scanner data. Vol. XXXI, *International Archives of Photogrammetry and Remote Sensing*, pp. 383–388, Part B3.

Kraus, K. and Pfeifer, N., 1998. Determination of terrain models in wooded areas with airborne laser scanner data. *ISPRS Journal of Photogrammetry and Remote Sensing* 53, pp. 193–203.

Lee, H. S. and Younan, N. H., 2003. DTM extraction of lidar returns via adaptive processing. *IEEE Transactions on Geoscience and Remote Sensing* 41(9), pp. 2063–2069.

Li, S., 1995. *Markov random field modeling in computer vision*. Springer Verlag.

Lohman, P., Koch, A. and Schaeffer, M., 2000. Approaches to the filtering of laser scanner data. Vol. 33, *International Archives of Photogrammetry and Remote Sensing*, Amsterdam, pp. 540–547, Part B3.

Metaxas, D. N. and Kakadiaris, I. A., 2002. Elastically adaptive deformable models. *IEEE Transactions on Pattern Analysis and Machine Intelligence* 24(10), pp. 1310–1321.

Montagnat, J., Delingette, H., Scapel, N. and Ayache, N., 2000. Representation, shape, topology and evolution of deformable surfaces. Application to 3D medical image segmentation. Technical Report 3954, INRIA.

Sithole, G., 2001. Filtering of laser altimetry data using a slope adaptive filter. Vol. XXXIV-3/W3, *International Archives of Photogrammetry and Remote Sensing*, Annapolis, pp. 203–210.

Sithole, G. and Vosselman, G., 2003. Comparison of filtering algorithms. Vol. XXXIV-3/W3, *International Archives of Photogrammetry and Remote Sensing*, Dresden, pp. 71–78.

Sohn, G. and Dowman, I., 2002. Terrain surface reconstruction by use of tetrahedron model with the MDL criterion. *International Archives of Photogrammetry and Remote Sensing*, Graz, pp. 336–244.

Vosselman, G., 2000. Slope based filtering of laser altimetry data. Vol. XXXIII, *International Archives of Photogrammetry and Remote Sensing*, Amsterdam, pp. 935–942, Part B3.

Zhang, K., Chen, S.-C., Whitman, D., Shyu, M.-L., Yan, J. and Zhang, C., 2003. A progressive morphological filter for removing nonground measurements from airborne lidar data. *IEEE Transactions on Geoscience and Remote Sensing* 41(4), pp. 872–882.

Zinger, S., Nikolova, M., Roux, M. and Maître, H., 2002. 3D sampling for airborne laser data of urban areas. *International Archives of Photogrammetry and Remote Sensing*, Graz, Austria, pp. 418–423.